J. L. Mauer
H. C. Pfeiffer
W. Stickel

Electron Optics of an Electron-Beam Lithographic System

Abstract: This paper describes the electron optics of a practical scanning electron-beam lithographic system (EL1) that provides high-volume direct wafer exposure. The throughput limitation inherent in serial exposure is greatly reduced by exposing entire pattern segments with a shaped beam. The shaped-beam concept represents a combination of scanning and projection methods. Twenty-five image points are exposed simultaneously to increase the spot current accordingly over that of a Gaussian round-beam system that exposes one image point at a time. The higher total current could lead to intensified Coulomb interaction between beam electrons, causing excessive Boersch effect and additional aberrations. However, the imaging and deflection methods described here are shown, by theoretical and experimental means, to reduce both the effects of Coulomb interaction and the total aberration of the system. This results in improvement of the beam current and field coverage compared with those found in conventional systems.

Introduction

In recent years electron-beam lithography has evolved from exploratory work on a laboratory scale to the mass production of devices and masks [1]. Usually, pattern elements are drawn on electron-sensitive resist with a small electron beam. Scanning the beam under digital control makes it possible to achieve high pattern flexibility and to store and regenerate the data for each pattern.

An electron-beam system is practical for production only if it yields high throughput. Considerable effort has been directed toward minimizing the effects that limit throughput, such as wafer I/O, table movement, registration, field coverage, and exposure time. Throughput can be improved by projecting the entire pattern with an electron beam. With this projection method, however, some pattern flexibility is lost. Also, there is no means of making dynamic corrections for pattern distortions and other aberrations; such corrections can be incorporated into scanning systems.

This paper describes the electron-optical features of an advanced lithographic system, EL1, designed to yield high throughput while retaining the advantages of scanning methods. The design of the imaging and deflection, and a method of stabilizing the beam automatically, have been developed to overcome some of the limitations of scanning systems. The system described here is designed as a production tool; its main functions are automated for consistent and reliable operation. The operation of the column reflects the need for pattern accuracy and for the ability to overlay successive patterns.

The exposure rate of the system is improved by projecting a square spot, the size of the smallest pattern element, and scanning the surface of the wafer with it. Figure 1 illustrates the advantage of using a square beam rather than a Gaussian round beam of the same resolution. The greater area of the square beam exposes 25 image points at a time as compared with a single one in the Gaussian round-beam system, thus reducing the total exposure time.

This larger spot, however, contains a higher spot current, which in turn leads to intensified Coulomb interactions between the beam electrons, and thus to excessive Boersch effect and additional aberrations [2–4]. To reduce the aberrations caused by the high current and the large field, we developed the deflection arrangement shown in Fig. 2, with the yoke in the center of the projection lens.

The operating characteristics of the system, which result from the design considerations, are described in this paper. The following sections give a physical description of the electron-beam column and the method of beam formation, and an outline of the optical characteristics of the final lens.

EL1 column

• *Beam formation*

The column design is based on the use of a shaped-beam concept to simultaneously optimize the shape of the

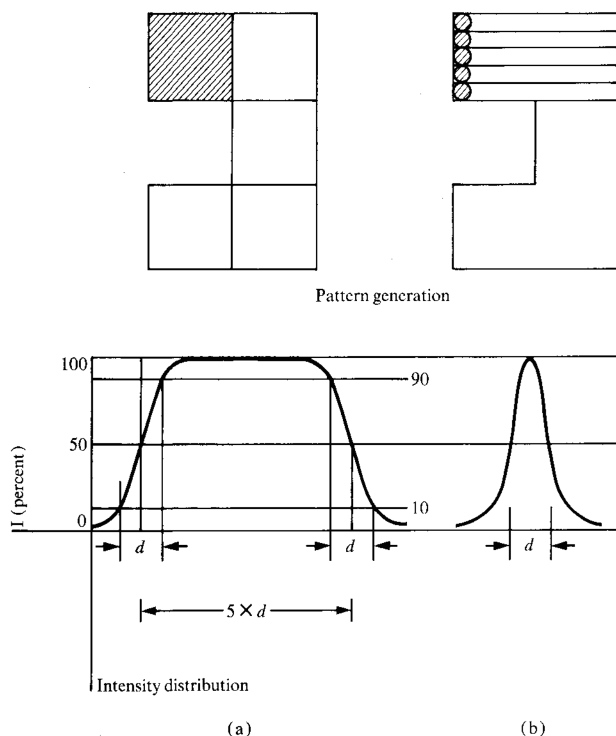

Figure 1 Square beam concept (a) vs round beam (b), where *d* represents the electron optical resolution of both concepts.

probe (size and edge slope) and the distribution of the probe current by implementing Koehler's [5] linked-beam tracing [6]. As Fig. 3 shows, the condenser lens images the source (gun crossover) into the entrance pupil of the demagnification section, providing the most efficient and uniform illumination of the probe (widely shaded tracing). The projection lens generates the probe by projecting a demagnified image of the object (square aperture) onto the target (narrow shading). The condenser and projection lenses act as conjugate elements in the sequential imaging of source and probe; the demagnification lenses establish the link between them.

The object, a hole 400 μm square in a thin metal plate, is irradiated by electrons from a tungsten-filament triode gun. (Pointed lanthanum boride emitters, though brighter, cannot be used because the illumination is nonuniform at the required brightness [7].) The image of the square aperture is demagnified in two steps almost down to the final probe size, 2.5 μm square. The first demagnification lens simultaneously creates a magnified image of the source in the plane of the beam-shaping aperture. The two apertures together provide an even current distribution by admitting only the center parts of both the emission cone (spot-shaping square aperture) and the source (beam-shaping round aperture).

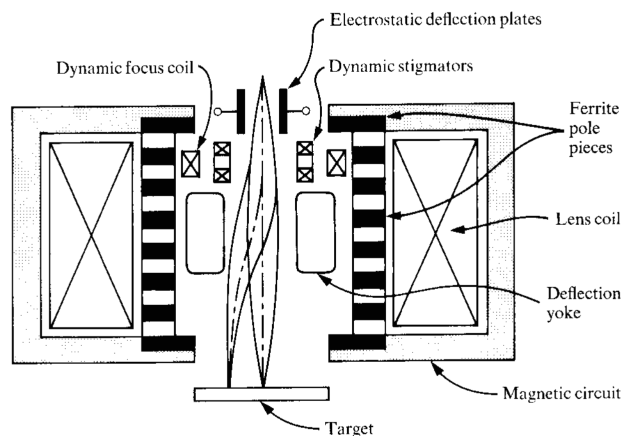

Figure 2 Schematic of projection lens with central deflection yoke.

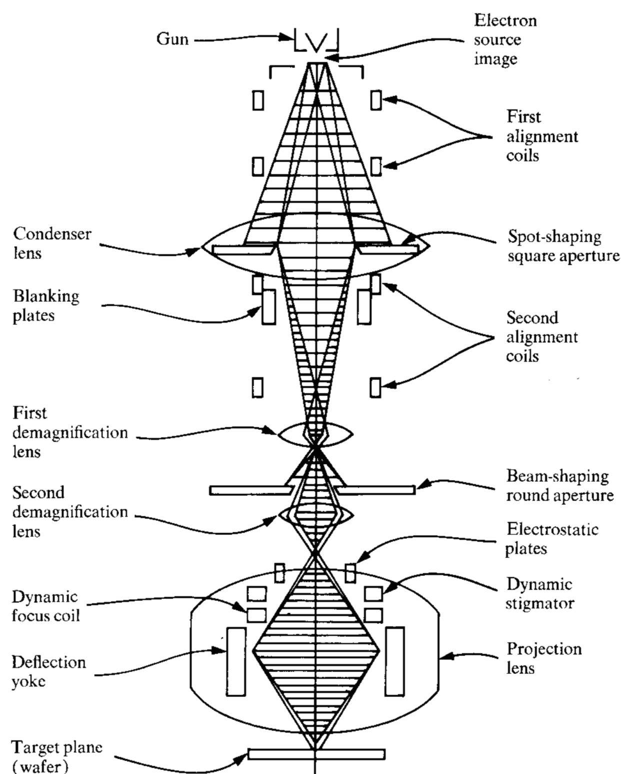

Figure 3 Column and components.

The second demagnification lens images the second aperture into the center of the projection lens, defining the semiangle of convergence. The use of a given aperture with a beam energy of 25 keV requires a brightness of 3×10^5 A/cm^2-sterad to achieve the specified target current, 3 μA. The final lens provides the necessary working distance to deflect the beam over the field to be exposed, 5 mm square. The beam is deflected by means of a toroidal yoke.

The projection lens is designed to accept coils for correcting defocus and astigmatism, and electrostatic deflection plates for applying small, fast positional corrections to the beam. The correction elements are placed above the deflection yoke, to avoid the field rotation and distortions that the corrective forces applied to the deflected beam would otherwise cause. Precautions have been taken to suppress the generation of eddy currents in the environment of the alternating magnetic deflection and correction fields; such eddy currents would affect the beam motion intolerably. Gold-coated insulating material is used for the deflection and correction components; the lens pole pieces are made of ferrite and are structured as shown in Fig. 2. Dynamic effects, which include eddy currents, cause less than 0.25 μm nonlinear distortions for a 5 $\times$ 5-mm field at nominal writing speed. These distortions are corrected as described below by taking advantage of the repetitive nature of the raster scan. Furthermore, each of the magnetic discs of the "sandwich" pole piece assumes a uniform magnetic potential, thus shielding the beam area from asymmetries in the lens coil.

For writing patterns, the intensity of the probe is modulated by electrostatic beam blanking. A pair of plates, close to the object, controls the illumination of the probe without spot movement at the target. Figure 3 shows all the essential elements of the column, and their locations. The gun contains a turret with 16 tungsten filaments, which makes possible virtually continuous operation for weeks. The beam is aligned with the apertures by sets of deflection yokes in the first and second alignment sections. The square aperture can be rotated mechanically to align its edges to the deflection axes; the heat from the beam minimizes contamination. The second aperture is adjusted laterally so that the beam passes through the optical center of the projection lens; it is heated externally. The stigmator coils are centered mechanically to the optical axis to prevent the beam from moving laterally during correction for astigmatism. The electrostatic plates can be rotated to match the axes of magnetic deflection. All the mechanical adjustments are performed from outside the vacuum with the column operating.

Most column components fit into sturdy sections 25 cm in diameter, made of soft magnetic material which, supported by μ-metal cylinders inside the alignment sections, protects the beam against external electromagnetic interference. The design of the lenses, optimized for low power dissipation, provides elasto- and thermomechanical stability.

• *Probe stabilization*

In order to apply the electron optical system to microfabrication, the electron probe must be stabilized. The two-dimensional beam-current distribution at the target has to be maintained over one or more pattern-writing periods, depending on how much time is allocated for readjustments.

The spatial current distribution is determined by size, squareness, uniformity, edge sharpness (slope), and total current. These properties require that the operating parameters of the lens, the alignment sections, the gun, and the correction devices be properly adjusted and stabilized in time and over the field to be exposed.

Three kinds of stabilization requirements can be identified:

a. Time-independent compensation of focus and astigmatism in synchronism with the beam deflection across the field: *dynamic corrections*, applied continuously.
b. Time-varying, column-related probe quality maintenance: *beam stabilization*, applied whenever required or convenient; for example, when the target table is being moved.
c. Time-varying adjustment of beam motion, both column-related and target-related: *deflection corrections*. Target-related deflection corrections (registration [8]) are performed before each pattern exposure, to correct for variations in the geometry and placement of the target. Deflection corrections for field distortions [9] are performed less often, as needed.

Dynamic correction is required to maintain a resolution of 10000 lines/field over a field 5 mm square, since edge slope of the probe deteriorates with increasing deflection of the beam away from the optical axis. Of the large variety of electron-optical aberrations composing the edge slope, field curvature can readily be compensated with axial electromagnetic fields, and astigmatism with lateral ones. These errors vary with the deflection angle, necessitating corrections that depend on the momentary position of the beam. Consequently, the corrective currents are fed to the magnetic compensation devices (focus and stigmatic coils) by hardware function generators activated in synchronism with the beam deflection. The optical concept, design, and machining accuracy allow those functions to be very simple. They are adjusted only once, during initial alignment; the spot shape is measured by scanning the beam over a reference target consisting of a network of thin crossed wires. The transmitted beam current is then picked up by a solid-state detector. The signal is either differentiated to show the spot cross section in two lateral dimensions, or processed to compute and optimize the edge slope.

Beam stabilization is required to correct for changes in gun conditions due to aging of the electron source, for thermal drifts of column and electronic components, and

for environmental changes both inside the vacuum (charging) and outside it (electromagnetic interference). A complex system of closed-loop control circuitry (servos) is implemented to maintain the edge slope, uniformity of illumination, and total current of the probe [10].

To explain the function of the servos, the tracings for both probe illumination and imaging are shown separately in Fig. 4. Brightness, gun, and alignment servos, being interrelated, are operated as a group. Since continuous adjustment [11] might interfere with pattern writing, the beam is adjusted off line during table moves.

During the servo actions, the beam is magnetically deflected to an off-center aperture in the same plate as the second, beam-shaping round aperture. The sample aperture plate underneath collects the current, to provide the reference for all three circuits.

The gun servo centers the beam to the spot-shaping square aperture, the alignment servo to the off-center aperture. The brightness servo compares the value of the collected current with a reference value, and adjusts the gun by controlling the filament temperature rather than the emission. Figure 5 demonstrates the advantage of the mode of operation applied here (point A) over conventional operation in the region of space-charge-limited emission (point B). The emission current must be stabilized to keep the gun operating in the plateau region of the brightness-emission curves, where the brightness is a definite function of the filament temperature. Thus optimum use is made of the filament, whereas at point B the filament is constantly overheated.

These servo actions lead to excellent performance. The total probe current is stabilized within ±1 percent of the specified value, 3 μA. The spot illumination is uniform to well within five percent. The filament has a lifetime of 30 to 40 hours at a brightness of 3×10^5 A/cm^2-sterad for a beam energy of 25 keV.

The focal plane is automatically stabilized with the focus servo, which maintains the minimum edge slope of the spot. The edge slope is measured by the same scanning method used in adjusting the dynamic corrections. The accuracy of the focus stabilization far exceeds the practical requirement defined by the depth of focus of the system.

Deflection corrections are introduced first to rectify nonlinear probe movement and thus establish a nominal deflection field, and then to adapt the nominal field to the position and shape of the individual target field.

Column-related distortions of the beam are caused by instabilities similar to those affecting the beam above the apertures, and by deviations due to electronic nonlinearities, residual eddy currents, and electron-optical displacement. A calibration procedure is initiated as often

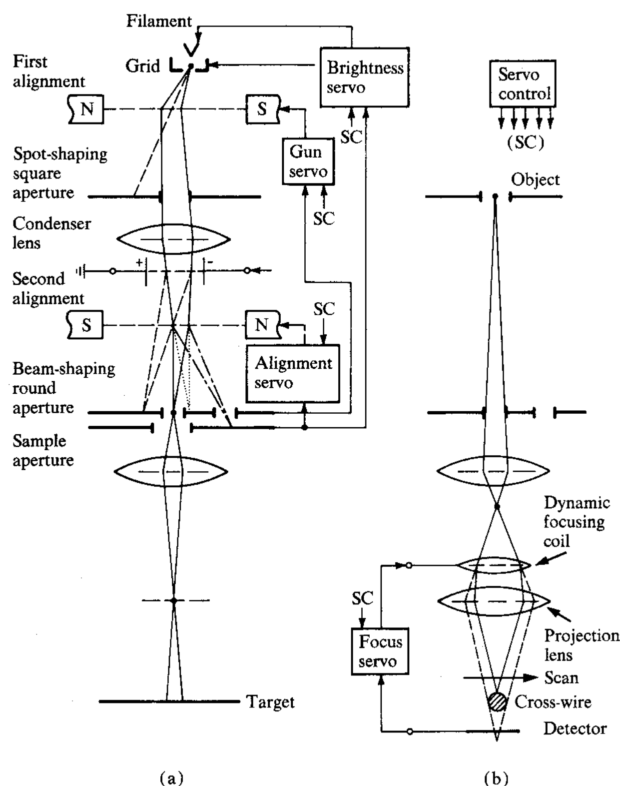

Figure 4 Beam tracing and stabilization. (a) Illumination. (b) Imaging.

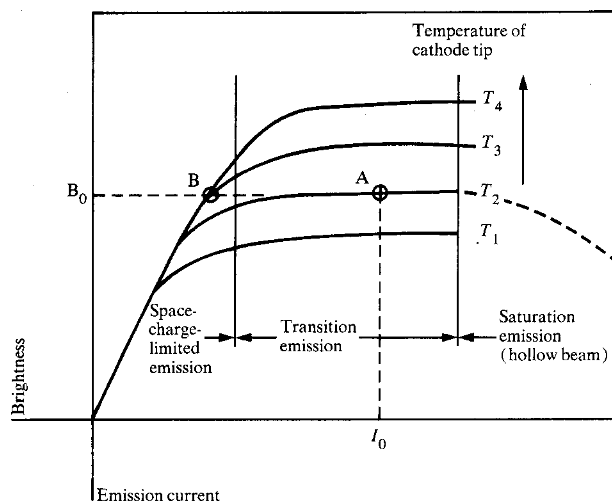

Figure 5 Gun operation concept.

as is deemed necessary to measure those deviations with reference to a target grid of known dimensions. Corrections are then applied to the input of the yoke to establish the nominal deflection.

Differences between the nominal field and the actual area to be exposed on the wafer are due to inaccurate table positioning, wafer warp, and variations in wafer

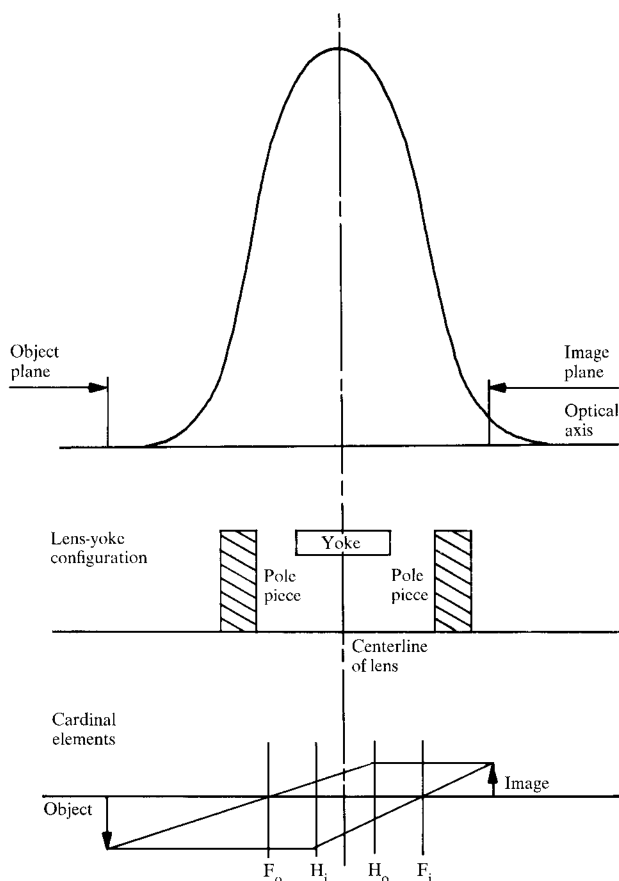

Figure 6 Axial magnetic field of the projection lens.

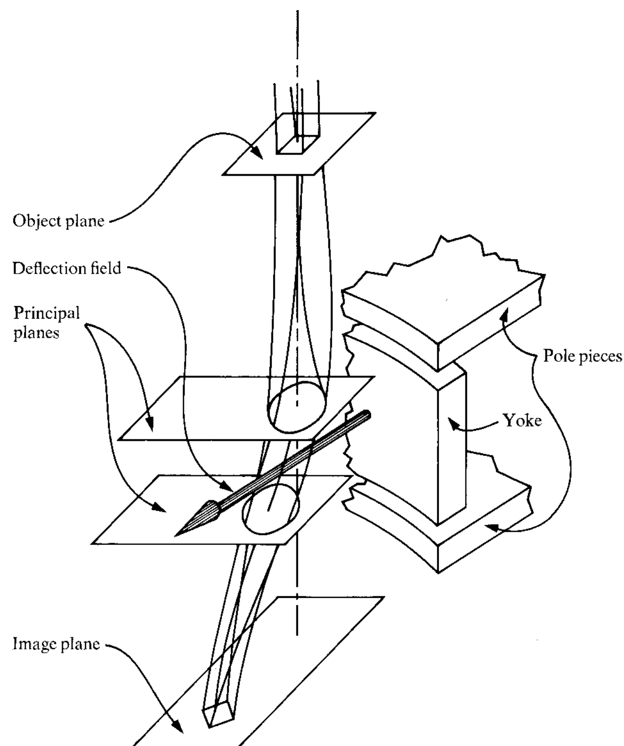

Figure 7 Calculated trajectory of the deflected beam.

thickness. For registration, they are detected by scanning the beam over topographic marks in the four corners of each field and evaluating the backscattered electron signals for the location of those marks. Corrections are applied to electrostatic plates to compensate for field shift, rotation, size change, and linear distortion. The probe defocusing caused by misplacement of the wafer surface from the nominal image plane is corrected by using the field-size-error signal to adjust the current in the dynamic focus coil, extending the range of the depth of focus.

Optical characteristics

• *Beam interaction*

The shaped-beam concept and the corresponding high total beam current result, as was mentioned earlier, in excessive electron-electron interactions. By accumulation, these Coulomb-scattering events can cause significant changes in momentum and energy along the electron beam. Such changes result in increased energy spread around the mean beam energy, as well as image deterioration caused by electron displacement and disorientation.

The total beam current is largest in the electron gun area, but blurring here has little effect except on the resultant brightness. More significant is the creation of energy spread in the gun region, known as the Boersch effect [12]. This effect gives rise to substantial chromatic aberration as the beam passes through yoke and projection lens.

Although the beam current in the projection lens is too small to increase the energy spread appreciably, it is large enough to blur the shaped spot in the image plane. A simple model of the electron-electron interaction serves to demonstrate the direct effect of this aberration on the design of the projection lens. The starting point of the model is a Monte Carlo calculation, initially developed by Loeffler [2], of electron-pair scattering in a beam. In this model, the median of the absolute trajectory displacement D is given by [3]

$$D \propto \frac{\Gamma(\lambda \alpha L)}{V\alpha^2}, \qquad (1)$$

where V is the beam energy in electron volts, α is the beam semiangle of convergence in radians, λ is the axial electron density of the beam, and L is the length of the interaction region.

For the high current of the shaped-beam system for which the dimensionless parameter $\lambda\alpha L$ is greater than unity, the function Γ becomes

$$\Gamma \propto (\lambda\alpha L)^{\beta}. \tag{2}$$

By appropriately substituting m, the angular magnification, and l, the distance between the object plane and the image plane, we get

$$D \propto \frac{i^{\beta} l^{\beta}}{\alpha^{2-\beta}} f(m), \tag{3}$$

where i is the beam current. The displacement reaches its minimum for a magnification just below unity.

Two distinct criteria for the lens are derived from Eq. (3): a foreshortened distance between object and image plane, and a magnification just below unity. Both favor a compact arrangement of projection lens and deflection yoke. By centering the yoke in the gap of the projection lens, the total aberrations are minimized. Superimposing the lens and deflection fields has the distinct advantage of making it possible to compensate the chromatic deflection error by the opposed lens dispersion, so that even the relatively large energy spreads of the high-brightness, high-current beams can be tolerated.

- *Imaging and deflection*

Because the projection lens is constructed from two widely spaced pole pieces, its magnetic field has a broad distribution along the optical axis (Fig. 6). The object plane is well outside it; the image plane is just within, near the lower pole piece. The linear magnification is 0.67.

The electron beam rotates about its own axis by 111° as it passes through the projection lens. When it is deflected (see the calculated trajectory in Fig. 7), the beam axis also rotates by an angle of 58°, measured from the initial direction of deflection. The principal planes of the lens extend 15 mm on either side of lens center; the focal length is 55 mm.

Further analysis of the beam trajectories provides the background for optimizing the design and arrangement of the lens and the yoke.

The third-order geometrical aberrations are calculated from a direct expansion about the optical axis. If the lens and deflection fields are superimposed, the expansion gives eight cylindrically symmetric terms and six fourfold terms; the fourfold terms are due to the quadrupole symmetry of the deflection field [13]. The yoke is so designed that all fourfold aberrations are eliminated, provided that the mechanical tolerances are tight enough.

The chromatic aberrations are calculated from the first-order terms of an expansion about the optical axis and the beam energy. The axial chromatic aberrations are independent of the yoke field; transverse chromatic aberrations are directly related to the deflection distance [13].

Table 1 Geometric and chromatic aberrations of EL1.

$\alpha_{max} = 7.5 \times 10^{-3}$ rad
R = 3.535 mm
$\Delta E = 7.5$ eV

Displacement (μm)	
Isotropic distortion	1.71*
Anisotropic distortion	−0.35*
Isotropic coma	0.02*
Anisotropic coma	0.04*
Aberration (μm)	
Field curvature	1.67*
Field curvature, spherical	0.46*
Isotropic astigmatism	0.49*
Anisotropic astigmatism	0.03
Isotropic coma	0.02
Anisotropic coma	0.04
Spherical	0.04
Isotropic transverse chromatic	0.11
Anisotropic transverse chromatic	0.36
Axial chromatic	0.15

*Correctable

The beam semiangle α has a distribution of values over the electron beam. Since using the maximum α in calculating aberrations leads to overestimates, the terms of the expansions are averaged over all possible values of α. For a given deflection, the mean of all trajectory displacements is the expected beam movement; the variance is a measure of the edge resolution of the spot.

Values of the various aberration components are given in Table 1. The averages are taken by using a truncated Gaussian distribution with an α limit of 7.5 mrad; the beam is deflected to the corner of a field 5 mm square. The energy spread is set at 7.5 eV, a representative value for the system; the actual value depends critically on the conditions in which the electron gun is operated.

Values of field curvature and isotropic astigmatism for this system are too large for the spot size and resolution specified. Therefore, as has been explained, these aberrations, including the term for the correlation between field curvature and spherical aberration, are dynamically corrected.

Distortion and, to a certain extent, coma (another aberration), are compensated by slight changes in the deflection. Much of the coma causes movement rather than decreased resolution.

Calculated values of the aberrations have been verified experimentally by measuring the edge slope of the spot, which is a known function of the aberrations. To

Table 2 Comparison of imaging and deflection systems for the corner of 5-mm square field.

	In-lens deflection			*Conventional SEM pre-lens double deflection*			*Improved double deflection*		
	(a)	(b)	(c)	(a)	(b)	(c)	(a)	(b)	(c)
Semi-angle (mr) maximum	7.5	5.0	5.0	7.5	5.0	5.0	7.5	5.0	5.0
Energy spread (eV)	7.5	2.5	2.5	7.5	2.5	2.5	7.5	2.5	2.5
Beam current (μA)	3.0	0.5	0.025	3.0	0.5	0.025	3.0	0.5	0.025
Field curvature (μm)	1.67	1.12	1.12	3.55	2.37	2.37	0.39	0.26	0.26
Field curv.—spherical (μm)	0.46	0.16	0.16	1.56	0.72	0.72	0.11	0.07	0.07
Isotropic astigmatism (μm)	0.49	0.33	0.33	1.45	0.97	0.97	0.23	0.16	0.16
Anisotropic astigmatism (μm)	0.03	0.02	0.02	0.20	0.13	0.13	0.15	0.10	0.10
Isotropic coma (μm)	0.02	0.01	0.01	0.04	0.03	0.03	0.01	0.01	0.01
Anisotropic coma (μm)	0.04	0.02	0.02	0.20	0.14	0.14	0.01	0.01	0.01
Spherical (μm)	0.04	0.01	0.01	0.38	0.12	0.12	0.02	0.01	0.01
Isotropic trans. chr. (μm)	0.11	0.04	0.04	0.51	0.17	0.17	0.06	0.02	0.02
Aniso. trans. chr. (μm)	0.36	0.12	0.12	0.57	0.19	0.19	0.06	0.02	0.02
Axial chr. (μm)	0.15	0.03	0.03	0.14	0.09	0.09	0.02	0.01	0.01
Interaction (μm)	0.28	0.09	0.00	0.78	0.27	0.00	0.78	0.27	0.00
Total before correction (μm)	1.87	1.19	1.19	4.34	2.70	2.68	0.93	0.43	0.33
Total after correction (μm)	0.50	0.16	0.13	1.29	0.44	0.35	0.80	0.29	0.11

(a) 2.5-μm square spot
(b) 1.0-μm square spot
(c) 0.25-μm round spot

separate individual contributions, the system is manipulated to enhance a specific aberration. The edge slope is measured by determining the current density distribution of the shaped spot, as explained earlier. The current is collected beyond the target as the beam is swept across one of the wires of the reference grid; the top curve represents the differentiation of the current signal as it passes one edge of the wire, and is proportional to the current density distribution in one axis. Since the spot edge is parallel to the wire (and perpendicular to the scan), the edge slope, differentiated again in the lower curve, gives the distribution of electron trajectories in the image plane. This distribution is a superposition of all aberrations and is not affected by the Gaussian distribution of the source. The measurements are calibrated by relating the upper trace on the oscilloscope to the diameter of the wire.

Performance comparisons

To illustrate the technological advance of the imaging and deflection concept described, the EL1 column has been compared to a more conventional SEM-type double-deflection system and an improved double-deflection system [14], all with the same beam current. The comparisons are summarized in Table 2, where spot size and shape are used as parameters to make the effect of the interaction aberration clear.

The total geometric and chromatic aberrations, calculated from the expansions, reflect the proper average over the semiangle of convergence. Interaction is calculated from the functional form of Eq. (1), calibrated by experiments. The total aberration is a quadrature sum of the interaction and the geometric and chromatic term. The total aberration after dynamic corrections are estimated by taking field curvature and isotropic astigmatism as zero.

The beam energy spread and the semiangle of convergence are related to the type of electron gun used. A lanthanum hexaboride (LaB_6) gun, with its lower energy spread and its higher brightness concentrated in a narrow emission cone, is used for the smaller spots. A tungsten gun, though limited in brightness and burdened with a higher energy spread, is used for the 2.5-μm spot because it illuminates the larger spot more uniformly.

The data for both double-deflection systems, as reported by Munro [14], have been reanalyzed to reflect the proper average over the semiangle and the different energy spreads. Movement due to coma has been removed from the aberrations, because it does not affect the resolution of the spot; the aberrations due to interaction have been added.

Conclusion

A scanning electron-beam lithography system is suitable for high-volume direct wafer exposure. The throughput limitation inherent in serial exposure is greatly reduced by exposing entire segments of the pattern with a shaped beam. Beam current and field coverage are better than those obtained with conventional SEM-type systems, because deflection and projection are superimposed to

compensate and minimize aberrations. Automation of all the vital system functions makes the system easy to operate and guarantees the necessary consistency in performance.

Acknowledgments

The authors gratefully acknowledge the contributions of M. Perkins to the design of the column control unit. They also thank E. Munro for allowing the use of his lens field programs.

References

1. G. L. Varness, D. F. Spicer, A. C. Rodger, and R. D. Holland, "High Speed Electron Beam Pattern Generation," *Proceedings of the Sixth International Conference on Electron and Ion Beam Science and Technology*, San Francisco, 1974, p. 97.
   D. R. Herriot, R. J. Collier, D. S. Alles, and J. W. Stafford, "EBES: A Practical Electron Lithographic System," *IEEE Trans. Electron Devices* **ED-22,** 385 (1975).
   P. F. W. Pease, J. P. Ballantyne, R. C. Henderson, A. M. Voschenkov, and L. D. Yau, "Applications of the Electron Beam Exposure System," *IEEE Trans. Electron Devices* **ED-22,** 393 (1975).
   T. H. P. Chang, "Instrumentation for Electron Beam Lithography," *IEEE Trans. Magnetics* **MAG-10,** 883 (1974).
   J. P. Beasley and D. G. Squire, "An Electron Beam Maskmaker," *IEEE Trans. Electron Devices* **ED-22,** 376 (1975).
   J. Trotel, "The Use of an Electron Beam Pattern Generation," *Extended Abstracts, Sixth International Conference on Electron and Ion Beam Science and Technology*, San Francisco, 1974, p. 505.
2. K. H. Loeffler, "Energy-Spread Generation in Electron-Optical Instruments," *Z. Angew. Phys.* **27,** 145 (1969).
3. K. H. Loeffler and R. H. Hudgin, "Energy-Spread Generation and Image Deterioration by the Stochastic Interaction Between Beam Electrons," *Proceedings of the Seventh International Conference on Electron Microscopy*, Grenoble, France, 1970, p. 67.
4. H. C. Pfeiffer, "Basic Limitations of Probe Forming Systems Due to Electron-Electron Interaction," *Proceedings of the Fifth Annual Scanning Electron Microscopy Symposium*, Chicago, 1972, p. 113.
5. A. Koehler, *Z. Wiss. Mikroskopie* **10,** 433 (1893).
6. H. C. Pfeiffer and K. H. Loeffler, "A High Current Square-Spot Probe for Micro Pattern Generation," *Proceedings of the Seventh International Conference on Electron Microscopy*, Grenoble, France, 1970, p. 63.
7. W. Stickel and H. C. Pfeiffer, "Emission Characteristics of the LaB_6 Electron Gun," *Proceedings of the Twelfth Symposium on Electron, Ion, and Laser Beam Technology*, Cambridge, MA, 1973, p. A15.
   A. N. Broers, *Proceedings of the Twelfth Symposium on Electron, Ion, and Laser Beam Technology*, Cambridge, MA, 1973, p. 979.
8. D. E. Davis, R. D. Moore, M. C. Williams, and O. C. Woodard, "Automatic Registration in an Electron-Beam Lithographic System," *IBM J. Res. Develop.* **21,** 498 (1977, this issue).
9. H. Engelke, J. F. Loughran, M. S. Michail, and P. M. Ryan, "Correction of Nonlinear Deflection Distortion in a Direct Exposure Electron-Beam System," *IBM J. Res. Develop.* **21,** 506, (1977, this issue).
10. S. Doran, M. Perkins, and W. Stickel, "Automatic Stabilization of an Electron-Probe Forming System," *J. Vac. Sci. Technol.* **12,** 1174 (1975).
11. F. Kurzweil, R. R. Barbar, and M. H. Dost, *Proceedings of the Ninth Symposium on Electron, Ion, and Laser Beam Technology*, Berkeley, CA, 1967, p. 350.
12. J. Boersch, "Experimentelle Bestimmung der Energieverteilung in Thermisch Ausgelösten Elektronenstrahlen," *Z. Phys.* **139,** 115 (1954).
13. E. Munro, "Calculation of the Optical Properties of Combined Magnetic Lenses and Deflection Systems With Superimposed Fields," *Optik* **39,** 450 (1974).
14. E. Munro, "Design and Optimization of Magnetic Lenses and Deflection Systems for Electron Beams," *J. Vac. Sci. Technol.* **12,** 1146 (1975).

Received February 1, 1977

The authors are located at the IBM System Products Division laboratory, East Fishkill (Hopewell Junction), New York 12533.